Crockford, P., et al., 2021, Reconstructing Neoproterozoic seawater chemistry from early diagenetic dolomite: Geology, v. 49, https://doi.org/10.1130/G48213.1

GSA Data Repository:

Reconstructing Neoproterozoic seawater chemistry from early diagenetic dolomite

Peter Crockford[1,2], Marcus Kunzmann[3], Clara Blättler[4], Boriana Kalderon-Asael[5], Anne-Sofie Ahm[2], Jack Murphy[2], Shlomit Sharoni[1], Galen Halverson[6], Noah Planavsky[5], Itay Halevy[1], John Higgins[2]

[1]Weizmann Inst. of Science, 76100, Israel
[2]Dept. Geoscience, Princeton University, NJ, 08544, USA
[3]CSIRO, Kensington, WA 6151, Australia
[4]Dept. Geophysical Sciences, University of Chicago, IL, 60637, USA
[5]Dept. Geology and Geophysics, Yale University, CT, 06511, USA
[6]Dept. Earth and Planetary Sciences, McGill University, QC, H3A 0E8, Canada

Supplementary Information

Isotopic notation

All isotopic measurements are presented in delta notation following equation S1:

$$(S1)\ \delta^{i}M = ((R_{sample}/R_{standard}) - 1) \times 1000$$

Where superscript *i* represents 44/40, 26, 13, 18, 7 and *M* represents elements C, O, Mg, Ca, Li and R represents isotopic ratios $^{44}Ca/^{40}Ca$, $^{26}Mg/^{24}Mg$, $^{13}C/^{12}C$, $^{18}O/^{16}O$, and $^{7}Li/^{6}Li$.

Carbon and oxygen isotopes

In total, 66 samples were measured for carbon ($\delta^{13}C$) and oxygen ($\delta^{18}O$) isotopes from the Coppercap Fm. Samples were first cut and then fresh surfaces were drilled with efforts made to avoid small veins. With a Nu-Carb device, between 100-140 µg of drilled powders were then dissolved in glass vials through the addition of H_3PO_4 at 70˚C. Liberated $CO_{2(g)}$ was then cryogenically isolated and analysed in dual-inlet mode on a Nu Perspective isotope ratio mass spectrometer at McGill University. Isotopic ratios were measured against an in-house reference gas and results are reported on the Vienna-Pee Dee Belemnite (V-PDB) scale. Uncertainty on measurements (1σ) based on the long-term analyses of NCM and UQ-6 standards is < 0.05‰.

Calcium and magnesium isotopes

Sample preparation

In total, 61 samples were measured for calcium isotopes ($\delta^{44/40}Ca$) and 66 samples were measured for magnesium isotopes ($\delta^{26}Mg$) in the Coppercap Fm. Carbonate powders

from the same aliquots utilized for carbon and oxygen isotopes were first weighed into 5 mg portions and placed into cleaned 15 mL Corning centristar tubes. Samples were then dissolved into 0.1 N buffered acetic acid ammonium hydroxide solution over four hours in a sonicator. Samples were then centrifuged and aliquots of the supernatant were transferred into cleaned 15 mL Corning centristar tubes. Aliquots of the bulk supernatants were then diluted ~30 times and calcium and magnesium were separated in different runs via a Thermo-Dionex ICS-5000+ ion chromatograph equipped with a fraction collector. Resultant calcium separates were then dried down and redissolved into concentrated distilled nitric acid. Samples were then dried down and taken back up into a volume of 2% nitric acid with the aim of having final solutions with a calcium concentration of 2 ppm.

Mass spectrometry

Calcium and magnesium isotopic ratios were measured at Princeton University using a Thermo Neptune plus multi collector inductively coupled plasma mass spectrometer (MC-ICPMS). Samples were introduced via an ESI Apex-IR sample introduction system. For calcium isotopes, $^{44}Ca/^{42}Ca$ isotopic ratios were measured through sample-standard bracketing and were performed in medium resolution mode to avoid isobaric $^{87}Sr^{2+}$ and $ArHH^{+}$ interferences. Under an assumption of no radiogenic ^{40}Ca excess (Caro et al., 2010), $^{44}Ca/^{40}Ca$ isotopic ratios were calculated utilizing established kinetic fractionation laws (2.05; Young et al., 2002) and are presented relative to modern seawater. Based on the long-term measurement of SRM-915b (n = 199) we report an external reproducibility (2σ) on measurements of 0.14‰ and obtained a value for SRM-915b of 1.15‰ that is within error of previously published results (Heuser and Eisenhauer, 2008). Magnesium isotope ratios ($^{26}Mg/^{24}Mg$) were measured in low resolution mode and were also performed using sample standard bracketing. Results are presented relative to Dead Sea Magnesium (DSM-3). Long term external precision (2σ) on magnesium isotope results was determined through repeated measurements of the Cambridge-1 standard (-2.59 +/- 0.07‰ n = 19) and modern seawater (-0.82 +/- 0.14 ‰ n = 21). Both magnesium and calcium isotopic results are presented as delta values and all results were plotted in three isotope space ($^{26}Mg/^{24}Mg$ vs. $^{25}Mg/^{24}Mg$ and $^{44}Ca/^{42}Ca$ vs. $^{43}Ca/^{42}Ca$) to confirm that isotopic values fell within typical mass-dependent variability.

Lithium isotopes

Sample preparation

The sample preparation and column chemistry for lithium isotope analysis were performed in a PicoTrace class-10 clean laboratory at Yale University. Blank lithium levels for each batch of samples were monitored and found to be negligible, at 0.00 % of the lithium in samples and standards. Approximately 375 mg of carbonate powder from samples was utilized for Li isotope measurements. Powders were first leached in 1M ammonium acetate and washed twice in 2X MQ2 H_2O to remove the lithium adsorbed or bound to secondary minerals. Powders were then dissolved in three steps (4h, 2h and 10 minutes) into a 0.05N hydrochloric acid solution, each time the sample being centrifuged for 5 minutes at 4000 rpm. Each supernatant was then extracted into Teflon beakers, dried on a hot plate and redissolved

in 6N HCl. Acid splits were dried down and then dissolved in 1ml of 0.2N HCl before being loaded directly onto 2.7 ml Bio-Rad AG50W-X12 (200-400 mesh) cation exchange resin pre-cleaned with 6N HCl and 2X MQ2 H_2O and preconditioned with 0.2N HCl. Lithium was released from the cation exchange resin through the addition of 0.2N HCl. After drying samples down, 5% HNO_3 was added to the samples by first adding distilled HNO_3 (left sealed on a hotplate at 60 °C for 30 minutes) and then diluting it down with 2X MQ2 H_2O to the desired strength. A split of 100µl was taken out and then 900µl of 2X MQ2 H_2O was added to the splits and these solutions were used for lithium and sodium concentration checks in post column solutions.

Mass spectrometry

The lithium and sodium post column concentrations and the lithium isotopic composition were measured with a Thermo Finnigan Neptune Plus ICP-MS at Yale University. Lithium isotope data was collected at low resolution in 1 block, 50 cycles per block and 5 second integrations per cycle. For these measurements we used the standard-sample-standard bracketing technique using the L-SVEC standard and then calculated sample values based on the bracketing standard values. In order to monitor the long-term reproducibility of our procedure, standards were processed with each set of samples. A typical standard error of a single measurement is 0.16 ‰. Unprocessed standard was employed as a drift monitor throughout each run giving a long-term external precision of 0.2 ‰ (1 σ), *n*=147. Column duplicates of samples typically fall within 0.26 ‰ (n=19). Geostandards after column chromatography give the following values: L-SVEC = 0.08 ± 0.52 ‰ (2σ) (*n*=19), BHVO-2 = 4.46 ± 0.55 ‰ (2σ) (*n*= 18) and Atlantic Seawater = 31.25 ± 0.51 ‰ (2σ) (*n*=13). Given that most of the samples had very low lithium concentrations and the standards were prepared to match those concentrations, the observed error is higher than maximum achievable in high concentration samples.

Data Correlation

Throughout the main text we refer to $\delta^{26}Mg$, $\delta^{44/40}Ca$ and $\delta^{7}Li$ values covarying. We arrive at this description through performing a Spearman rank correlation test. This test is a non-parametric measure of the dependence of two variables. We specifically performed a Spearman test and not a Pearson test because we did not assume a Gaussian distribution of our data. In all cases, we found a statistically (95% CI) significant correlation between $\delta^{26}Mg$, $\delta^{44/40}Ca$ and $\delta^{7}Li$ values, which is why we use the term covariation in the main text.

Table S1: Spearman r correlation test

	Ca vs. Mg	Ca vs. Li	Li vs. Mg
r	-0.3971	-0.5192	0.6449
95% CI	-0.5964 to -0.1518	-0.6910 to -0.2919	0.4449 to 0.7837
P (two-tailed, approximate)	0.002	<.001	<.001
significant? (alpha = 0.05)	Yes	Yes	Yes
number of XY pairs	60	57	52

Description of diagenetic model

To constrain the origin of geochemical signatures in the Coppercap Fm., we model carbonate diagenesis and dolomitization using a numerical model of Ahm et al., (2018). Since the geochemistry of the original carbonate precipitates of the Coppercap Fm. is not known and because the initial model did not include Li, we modified the code of Ahm et al., (2018) to: 1) ensure the chemistry of initial precipitates is consistent with our proposed seawater composition and 2) added Li and Li isotopes into this modelling framework partially based on recent results from the Bahamas by Dellinger et al., (2020) (see Taylor et al., 2018 for an alternative view on the Li isotope fractionation factor into dolomite). This model provides predictions for the geochemistry of the diagenetic fluid. It arrives at such predictions by finding model solutions that provide the best fit to isotopic data from natural samples which we describe in more detail below.

The model simulates early marine carbonate diagenesis through the dissolution of primary calcium carbonate and re-precipitation of dolomite along a flow path. Again, a slight modification to the code of Ahm et al., (2018) was made to ensure that original precipitates form from a hypothesized seawater composition, which forms the basis of the diagenetic fluid that the original precipitates recrystallize and diagenetically alter within. Based on observations from modern carbonate platforms, we assume that the Coppercap Fm. was dolomitized during early marine diagenesis within 100,000 yrs and use a reaction rate of 0.01% kyr^{-1} and a fluid-flow rate of 0.1 m yr^{-1} (Table S2; Higgins et al., 2018). However, since we evaluate our model output in cross-plot space, our model results are not significantly affected by changes in either reaction rates or flow rates. Importantly, the model results with respect to lithium are sensitive to the choice of Li partition coefficient into dolomite which to date has not been experimentally determined at low temperatures. To achieve our best model fit we tuned this parameter finding a value of 0.0005, however, increasing it up to ≈0.0015 still provided good fits to the data. This 'best fit' partition coefficient range is potentially quite different from results of Dellinger et al., (2020) whose data could suggest a value closer to 0.008 in the Bahamas. While there are many possibilities for this potential difference including differences in seawater chemistry (or chemistry of the diagenetic fluid), temperature or partitioning calculations (cf., Langer et al., 2015; 2020), these results highlight the much-needed continued effort to constrain environmental controls on the lithium partition coefficient into dolomite.

The model outputs isotopic trajectories that represent mixtures of primary carbonates (with a calculated composition from the prescribed seawater composition; see Table S2) and diagenetic dolomites spanning a range of fluid- to sediment-buffered compositions. As a result, the model output is a ternary phase-space between pairs of geochemical proxies that is defined by the geochemistry of the primary sediment and fluid-buffered and sediment-buffered trajectories, which terminate at 100% diagenetically altered end-member solutions. By identifying the fluid- and sediment-buffered end-members that are consistent with data from 100% recrystallized samples (100% dolomite), we can use the model to infer the composition of the diagenetic fluid and, therefore, of the primary sediment. That is, we overlay data from the Coppercap Fm. and explore model solutions that can provide the best fit to the data, which then allow us to explore the geochemistry of the diagenetic fluid. To ensure consistent predictions of different proxies, the position and shape of the model phase space is

constrained by visually optimizing the percentage of alteration (+/- 20%) across all phase spaces. For example, samples that fall into the 100% dolomitized phase-space of $\delta^{44/40}Ca$ versus $\delta^{26}Mg$ values, should also near 100% dolomitization in the phase-space $\delta^{44/40}Ca$ versus $\delta^{7}Li$ values.

Samples that are less than 100% recrystallized in model phase spaces are interpreted to only be partially altered during early marine diagenesis (Higgins et al., 2018). These samples are subsequently stabilized during later burial diagenesis in conditions that are sediment-buffered (i.e., much lower water-rock ratios), thus preserving the geochemical signals associated with early marine diagenesis. That is, our model does not assume that samples do not undergo subsequent diagenetic recrystallization during burial, simply that this recrystallization must have been sediment-buffered and would therefore preserve the geochemical signature of early marine diagenesis and not further alter the chemistry of the carbonate away from this early diagenetic composition.

An important final note, overlaying data from natural samples on model solutions will not yield perfect agreement. In other words, given the specified chemical and isotopic compositions of the original mineral and a diagenetic fluid, the idealized model predictions will not always agree with fine details in the data. For example, minor differences are expected in the degree of alteration of specific samples between isotope cross-plots. More major departures from 90-100% dolomitization contours of samples that are known to be fully dolomitized suggest that alternative explanations should be explored. This is an additional strength of this approach as it allows for the identification of samples or sample-intervals that may have been subjected to either different conditions, or additional processes that the model is unable to capture in a single simulation.

Table S2: All model parameters.

Parameter	Definition	Value used in model	References
$\alpha_{Ca\text{-}Dol}$	Ca isotopic fractionation factor for dolomitization	1.000	Jacobsen and Holmden, 2008; Fantle and DePaolo, 2007
$\alpha_{Mg\text{-}Dol}$	Mg isotopic fractionation factor for dolomitization	0.9980	Fantle and Higgins, 2014
$\alpha_{C\text{-}Dol}$	C isotopic fractionation factor for dolomitization	1.0025	Horita, 2014
$\alpha_{Li\text{-}Dol}$	Li isotopic fractionation factor for dolomitization	1.000	Dellinger et al., 2020
$K_{Li\text{-}Dol}$	Li/Ca partition coefficient into dolomite	0.0005	-
$\alpha_{Ca\text{-}Arag}$	Ca isotopic fractionation factor for aragonite	0.9985	Gussone et al., 2020
$\alpha_{Mg\text{-}Arag}$	Mg isotopic fractionation factor for aragonite	0.9993	Wang et al., 2013
$\alpha_{C\text{-}Arag}$	C isotopic fractionation factor for aragonite	1.0027	Romanek et al., 1992
$\alpha_{Li\text{-}Arag}$	Li isotopic fractionation factor for aragonite	0.988	Marriott et al., 2004; Dellinger et al., 2018;

			Pogge von Strandman et al., 2019
$K_{Li\text{-}Arag}$	Li/Ca partition coefficient into aragonite	0.003	Dellinger et al., 2020
$K_{Mg\text{-}Arag}$	Mg/Ca partition coefficient for aragonite	0.0019	Ahm et al. 2018
R	Reaction rate	$1x10^{-5}$ yr^{-1}	Higgins et al., 2018; Swart et al., 1987
u	Fluid advection rate	0.01 m yr^{-1}	Henderson et al., 1999
M_f	Chemical composition of diagenetic fluid (mmol/kg)	Ca = 19.1, Mg = 43.2, Li = 0.002	Best-fit estimate in this study
M_s	Chemical composition of primary solid (aragonite)	Ca = 39.5%, C = 12%, Mg = 1.03%, Li = 0.03 ppm	Best-fit estimate in this study
δ_f	Isotopic composition of diagenetic fluid	$\delta^{44/40}$Ca = 0.0‰, δ^{26}Mg = 0.1‰, δ^{7}Li = 13‰	Best-fit estimate in this study
δ_s	Isotopic composition of primary solid (aragonite)	$\delta^{44/40}$Ca = -1.5‰, δ^{26}Mg = -0.6‰, δ^{7}Li = 1‰	Best-fit estimate in this study

Model fit to data from the Coppercap Fm.

Our ability to fit diagenetic model solutions with geochemical data (see main text) provides a compelling case for early marine diagenesis driving the majority of geochemical variability observed in the Coppercap Fm. This is seen in Fig. 2 of the main text, which is also replotted here as Fig. S1. In Fig. S1 it is shown that the upper and middle portions of the Coppercap Fm. predominantly plot within the 80-100% diagenetically altered contours between fluid and sediment buffered end-members, with the middle portion of the section clustering toward the fluid buffered end-member and the top of the section clustering toward the sediment buffered end-member in δ^{26}Mg - δ^{7}Li, δ^{26}Mg - $\delta^{44/40}$Ca and δ^{7}Li - $\delta^{44/40}$Ca cross-plot space. However, many lower section samples do not fall within the >80% diagenetically altered (dolomitized) field (Fig. S1). This observation of the lower samples can be explained by one of three different possibilities: 1) samples in the lower portion of the section are not completely dolomite and retain some of their original geochemistry and thus plot closer to the initial aragonite, 2) lower samples underwent a slightly different diagenetic history than samples above due to local shifts in fluid composition, or, 3) seawater chemistry changed and thus the diagenetic fluid and initial aragonite geochemistry shifted between the lower samples and the samples above. We can immediately rule out the first scenario, as all samples in the Coppercap Fm. are dolomite (Table S9). Below, we explore the second and third scenarios outlined above in detail.

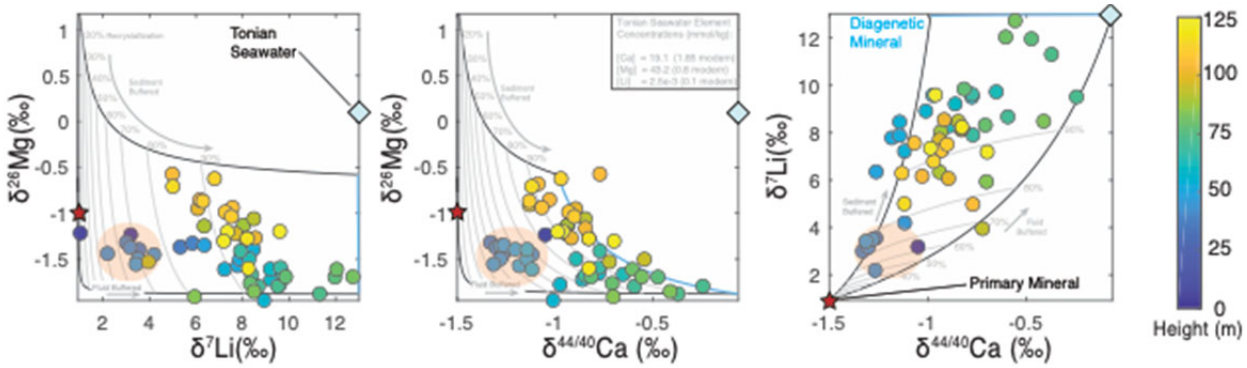

Figure S1: Figure 2 from the main text with δ^{26}Mg - δ^{7}Li, δ^{26}Mg - $\delta^{44/40}$Ca and δ^{7}Li - $\delta^{44/40}$Ca cross-plots of both model solutions and data from the Coppercap Fm. The colours of data points represent stratigraphic height. The primary mineral (aragonite) is represented by the red star, the blue line corresponds to the diagenetic product (dolomite) and the light blue diamond represents the composition of Tonian seawater. Upper black curves on the left two panels and the left curves on the right-most panel represent sediment buffered trajectories. Lower black curves on the left two panels and the right curve on the right most panel represents fluid buffered trajectories. Grey contours represent % recrystallization from the primary mineral to the diagenetic product. In the case of the Coppercap Fm. this corresponds to aragonite at 0% and stoichiometric dolomite at 100%, with minor element compositions corresponding to aragonite that precipitated from our prescribed seawater composition and dolomite geochemistry from the Coppercap Fm. The peach-coloured field highlights data points from the lower portion of the Coppercap Fm., which are dolomite but do not plot close to the diagenetic (dolomite) end-member mineral composition. Such a model-measurement misfit requires exploration of alternative explanations.

Changes in seawater chemistry on the required timescale are unlikely. We first consider the possibility that global seawater geochemistry shifted between the time of deposition of the lower samples to the time of deposition of the middle and upper samples in the Coppercap Fm. A change in seawater chemistry would have shifted the composition of the diagenetic fluid as well as shifted the original composition of the aragonite that we assume precipitated from it. Exploring diagenetic model phase spaces, we are able to generate solutions consistent with samples in the lower section (i.e., we can capture sample geochemistry within >80% dolomitized fields) by altering element concentrations in the diagenetic fluid (seawater) as well as its isotopic composition (Fig. S2). The most dramatic changes to fluid chemistry required are either through a reduction in [Ca] and/or a reduction in $\delta^{44/40}$Ca values of the diagenetic fluid that dolomitized lower samples compared to the diagenetic fluid composition required for model solutions for samples in the middle and upper portions of the section (Table S3). We primarily focus on Ca in the discussion below, as much less significant shifts in diagenetic fluid [Mg], [Li] and δ^{26}Mg values are required to achieve model fits.

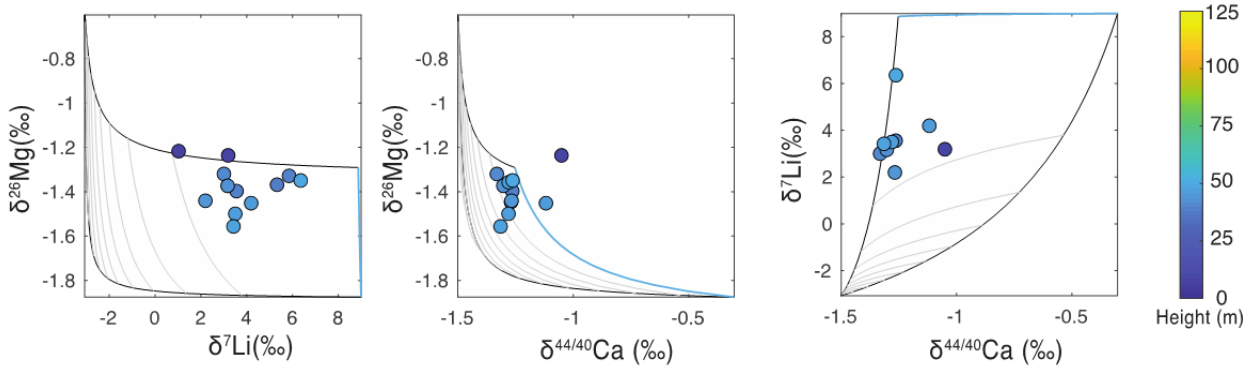

Figure S2: $\delta^{26}Mg$ - $\delta^{7}Li$, $\delta^{26}Mg$ - $\delta^{44/40}Ca$ and $\delta^{7}Li$ - $\delta^{44/40}Ca$ cross-plots of both model solutions and data from the lower portion of the Coppercap Fm. The colours of data points represent stratigraphic height which corresponds to the colour legend to the right of the figure. Model solutions correspond to parameters presented in table S3, which was a scenario to explore changing diagenetic fluid (seawater) element concentrations to seek out a model fit to the lower Copper cap samples.

Table S3: Model parameters to explain geochemistry of lower samples through changes in the chemical composition of seawater.

Parameter	Definition	Value used in model
M_f	Chemical composition of diagenetic fluid (mmol/kg)	Ca = 3.0, Mg = 32.4, Li = 0.002
M_s	Chemical composition of primary solid (aragonite)	Ca = 38%, C = 12%, Mg = 0.5%, Li = 0.13 ppm
δ_f	Isotopic composition of diagenetic fluid	$\delta^{44/40}Ca$ = 0.0‰, $\delta^{26}Mg$ = 0.1‰, $\delta^{7}Li$ = 13‰
δ_s	Isotopic composition of primary solid (aragonite)	$\delta^{44/40}Ca$ = -1.5‰, $\delta^{26}Mg$ = -0.8‰, $\delta^{7}Li$ = 1‰

Although permissible in our calculations, the required shift in seawater [Ca] would be from 3 mmol/kg in the lower section to 19 mmol/kg in the middle section (compare Tables S2 and S3). Because sedimentary facies do not dramatically change from the lower section to the middle section, we estimate the time captured across this transition by calculating a uniform deposition rate between previous geochronological constraints on the Coppercap Fm. and age-equivalent units and apply this depositional rate to the transition between lower samples and middle samples (Macdonald et al., 2010; Strauss et al., 2014; Rooney et al., 2014; MacLennan et al., 2017). With these constraints in place, it can be estimated that < 2 Myr is captured across this transition. Such a shift in [Ca] over the required timescale would not occur without significant implications for other aspects of the Earth system, which we discuss below.

The main sources of Ca to seawater is continental weathering of carbonate and silicate rocks and off-axis seafloor weathering reactions. The main removal mechanism of Ca from seawater is carbonate burial. An increase in the [Ca] of seawater could occur in response to an increase in Ca sources via enhanced weatherability or enhanced weathering rates, or a decrease in carbonate burial. Simply enhancing seawater [Ca] through increasing Ca input from continental or seafloor weathering (i.e., increasing weatherability) would lead to net CO_2 drawdown and a reduction in global temperature which would buffer against increasing marine [Ca] through the slowing of weathering rates, and we can rule out such a scenario.

Alternatively, maintaining a constant Ca input to the oceans, we can estimate the reduction in carbonate burial needed to cause a 16 mmol increase in seawater [Ca]. Taking modern input and burial values and an initial [Ca] of 3 mmol/kg, an approximate 50% reduction in carbonate burial would be required to induce the required 16 mmol/kg shift in [Ca] over < 2 Myrs. However, invoking a reduction in carbonate burial would ultimately lead to an increase in ocean alkalinity and drawdown of atmospheric CO_2, which would, in turn, reduce weathering rates and throttle the Ca supply. Therefore, this mechanism would require a CO_2 source concurrent with the reduction in carbonate burial. A massive injection of CO_2 into the ocean by large-scale organic matter respiration ($\delta^{13}C$ ~-25‰) or extreme volcanic outgassing ($\delta^{13}C$ ~-6‰) would cause a negative excursion in marine carbonate $\delta^{13}C$ values, inconsistent with the sedimentary record. Together these arguments weaken the case for a severe reduction in carbonate burial as a mechanism to increase seawater [Ca].

The above arguments leave enhanced volcanic CO_2 degassing as the only conceivable mechanism to dramatically increase [Ca] by ≈16 mmol/kg over our estimated time interval of < 2 Myrs (higher temperature increases weathering rates). The isotopic consequences of such an injection are discussed above. Additionally, this mechanism is likely to result in dramatic changes to other components of the Earth surface, from increases to global surface temperature to changes in primary productivity and organic carbon burial. These changes would likely leave unambiguous signatures somewhere in the sedimentary record. To illustrate this point, if we again consider an extreme imbalance in which increases to Ca inputs do not increase Ca outputs, we would need to nearly double the Ca input flux to the ocean over the < 2 Myr interval between the lower and middle portions of the Coppercap Fm. Such a doubling of inputs, as discussed above, can only be achieved through enhancement of global weathering rates that requires an increase in surface temperature in response to increases in pCO_2. Using estimates of the temperature dependence of weathering rates (e.g., Berner and Kothavala et al., 2001), such an increase in the Ca source would require approximately a doubling of atmospheric pCO_2. Such large, rapid shifts in atmospheric pCO_2 would likely require an extreme event, such as the eruption of a large igneous province (LIP). In the late Tonian a LIP eruption would be particularly necessary as it has been suggested that arc-volcanism was in a steady decline at this time (Mckenzie et al., 2016). However, geochronological constraints place the interval in question (between ≈735 -732 Ma), after notable events in the Tonian such as Katangan magmatism in the western Kalahari (~750 Ma), and before the eruption of the Franklin LIP (~723 Ma), making such a mechanism unlikely (Ernst et al., 2008). Finally, arguments above notwithstanding, it is important to note that such changes would require shifts in [Ca] to occur 1-2 orders of magnitude faster than documented across the Phanerozoic (Lowenstien et al., 2003; Horita et al., 2002). The above arguments make it difficult to justify invoking changes in silicate weathering to explain dramatic changes in seawater [Ca] between lower and middle portions of our section of the Coppercap Fm.

Changes in seawater isotopic composition are unlikely. Model-measurement agreement in the lower section can also be achieved by varying the isotopic composition of seawater. Maintaining consistent element concentrations between lower, middle and upper portions of the Coppercap Fm. we can achieve model fits for the lower samples within >80% dolomitized fields by lowering the $\delta^{44/40}Ca$ and $\delta^{7}Li$ values of seawater by 0.6 and 7‰ respectively (Table S4; Fig. S3).

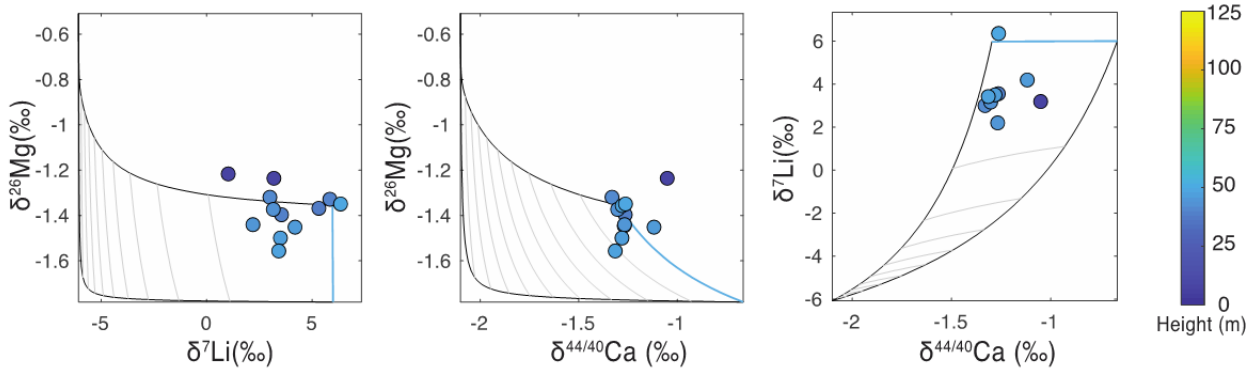

Figure S3: $\delta^{26}Mg$ - $\delta^{7}Li$, $\delta^{26}Mg$ - $\delta^{44/40}Ca$ and $\delta^{7}Li$ - $\delta^{44/40}Ca$ cross-plots of both model solutions and data from the lower portion of the Coppercap Fm. The colours of data points represent stratigraphic height. Model

solutions correspond to parameters presented in Table S4, which was a scenario to explore changing diagenetic fluid (seawater) isotopic compositions to seek out a model fit to the lower Coppercap Fm. samples.

Table S4: Model parameters to explain geochemistry of lower samples through changes in isotopic compositions of seawater.

Parameter	Definition	Value used in model
M_f	Chemical composition of diagenetic fluid (mmol/kg)	Ca = 19.1, Mg = 43.2, Li = 0.002
M_s	Chemical composition of primary solid (aragonite)	Ca = 39.5%, C = 12%, Mg = 1.03%, Li = 0.03 ppm
δ_f	Isotopic composition of diagenetic fluid	$\delta^{44/40}$Ca = -0.6‰, δ^{26}Mg = 0.2‰, δ^{7}Li = 6‰
δ_s	Isotopic composition of primary solid (aragonite)	$\delta^{44/40}$Ca = -1.5‰, δ^{26}Mg = -0.8‰, δ^{7}Li = 1‰

The needed shifts in seawater isotopic composition are potentially possible through increases to congruent silicate weathering, which would suppress Li isotope fractionation during continental weathering, as well as near-complete quantitative uptake of Li at the locations of Li-sinks, which would suppress isotopic fractionation associated with such processes. Additionally, a seawater δ^7Li value as low as 7‰ predicts that some marine carbonates at this time would bear δ^7Li < 0‰. Such low δ^7Li values have yet to be observed. In the case of Ca isotopes, lowering seawater $\delta^{44/40}$Ca values to -0.6‰ could be achieved through lowering the $\delta^{44/40}$Ca value of Ca inputs. This may be possible through weathering aragonite-dominated terrains exposed by dramatic sea level drop or through a non-steady state scenario where Ca inputs are not balanced by outputs, thereby shifting seawater $\delta^{44/40}$Ca values closer to the Ca input compositions. Such a shift would likely occur with some indication in sedimentary facies, which is not observed in our section. Furthermore, with likely $\delta^{44/40}$Ca values of the possible sources and sinks of Ca invoked to drive this change in seawater $\delta^{44/40}$Ca values, the required fluxes of Ca are themselves substantial. For example, suspending carbonate burial altogether and achieving the decrease in seawater $\delta^{44/40}$Ca values by weathering an aragonite platform, would increase [Ca] by almost 70%. If carbonate burial were ongoing, the time required for turnover of the marine Ca pool to affect a change of -0.6‰ would be long, relative to the time available in the Coppercap Fm. section. Therefore, arguments made above in the exploration of changes in [Ca] as the driver of the observed changes in the isotopic composition of diagenetic dolomite also weaken an explanation based on enhanced aragonite weathering. Even in a combined scenario (Table S5, Fig. S4), where we allow seawater to evolve isotopically and compositionally, the arguments presented above still apply, rendering such explanations difficult to support.

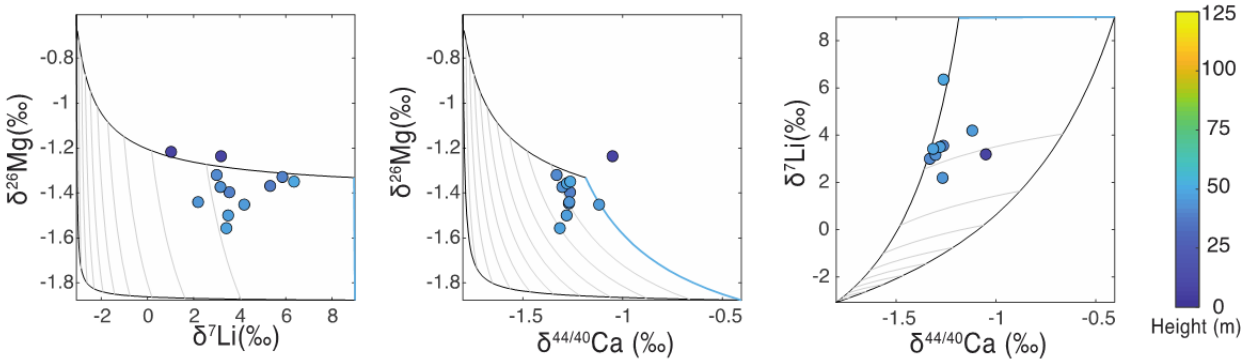

Figure S4: $\delta^{26}Mg$ - $\delta^{7}Li$, $\delta^{26}Mg$ - $\delta^{44/40}Ca$ and $\delta^{7}Li$ - $\delta^{44/40}Ca$ cross-plots of both model solutions and data from the lower portion of the Coppercap Fm. The colours of data points represent stratigraphic height. Model solutions correspond to parameters presented in Table S5, which was a scenario to explore changing diagenetic fluid (seawater) chemical and isotopic compositions to seek out a model fit to the lower Coppercap Fm. samples.

Table S5: Model parameters to explain geochemistry of lower samples through changes in the chemical and isotopic compositions of seawater.

Parameter	Definition	Value used in model
M_f	Chemical composition of diagenetic fluid (mmol/kg)	Ca = 11.1, Mg = 35.1, Li = 0.002
M_s	Chemical composition of primary solid (aragonite)	Ca = 39.5%, C = 12%, Mg = 1.03%, Li = 0.03 ppm
δ_f	Isotopic composition of diagenetic fluid	$\delta^{44/40}Ca$ = -0.3‰, $\delta^{26}Mg$ = 0.2‰, $\delta^{7}Li$ = 6‰
δ_s	Isotopic composition of primary solid (aragonite)	$\delta^{44/40}Ca$ = -1.5‰, $\delta^{26}Mg$ = -0.8‰, $\delta^{7}Li$ = 1‰

While we cannot definitively rule out the above scenarios, all make predictions for extreme changes in seawater chemistry across a < 2 Myr interval that should be expressed globally. Moreover, such scenarios come along with additional implications beyond the cycles of Ca, Mg and Li. As it is difficult to point to any obvious causes of such dramatic shifts, we explore an alternative local explanation below.

A different diagenetic fluid may explain the isotopic composition of the lower section. To explore a scenario where seawater chemistry did not significantly change across the deposition of the Coppercap Fm., we maintain the same initial aragonite geochemistry but alter the composition of the diagenetic fluid that dolomitized the samples in the lower portion of the section (Tables S6, S7 and S8). The best model fit to the data is achieved with a fluid with lower Ca, Mg and Li concentrations and lower $\delta^{44/40}Ca$, $\delta^{26}Mg$ and $\delta^{7}Li$ values than the proposed Tonian seawater (Table S8).

To deduce the origins of such a fluid we first consider the possibility that lower section samples were diagenetically altered by a fluid that formed through the dilution of seawater with meteoric fluids. However, since Li would only be sourced from seawater in this case, the concentration and isotopic composition of Li in the meteoric-seawater mix do not allow reproduction of the full range of observed $\delta^{7}Li$ values in model end-products that are >80% dolomite, as required in the case of the Coppercap Fm. samples, which are fully dolomitized.

In the second case we consider a scenario where lower samples were dolomitized by a fluid that formed through a mixture of seawater and terrestrial groundwaters at aragonite

saturation (Table S6). We first envision terrestrial groundwater flowing through an aragonite aquifer, reaching saturation with the aragonite and then mixing with seawater at a freshwater-seawater interface. We assign a Ca concentration and isotopic composition consistent with aragonite dissolution until saturation is reached, and concentrations and isotopic compositions of Mg and Li that reflect release from dissolving aragonite. The best-fit solution in this case is also incapable of reproducing the range of observed δ^7Li values in model end-products that are >80% dolomite (Fig. S5). Even in the case where we modify the chemistry of waters that flowed into the aquifer allowing for different Ca:Mg:Li ratios (inferred from modern riverine measurements flowing through silicate-dominate terrains; e.g., Tipper et al., 2012), we are still unable to achieve a satisfactory model fit (Fig. S6, Table S7). Specifically, even when modifying [Mg] and [Li] to ≈0.5 mM and 0.001 mM respectively (Table S7), many data points are unable to be captured in >80% dolomite fields of a model solution.

The final option that we consider is that lower section samples were dolomitized in a fluid that formed as mixture of seawater and a less saline fluid with approximately 2-3 times less Mg, Li and Ca than contemporaneous seawater and lower δ^7Li, δ^{26}Mg and $\delta^{44/40}$Ca compositions (Table S8). Such a scenario is potentially analagous to modern settings such as carbonate aquifers in Rottnest Island in Western Australia (Martin et al., 2020). Solutions generated from this scenario fall close to the sediment-buffered end-member trajectory and encapsulate most of the lower section data within model end-products that are >80% dolomite. Given the diversity of possible sources of a solution of intermediate salinity, and the possibility mixing between more than two end-member fluids, it is difficult to uniquely interpret this scenario. However, allodapic carbonate facies strongly imply a marine slope environment for original deposition of the lower section samples. In such an environment, the most likely solution with which seawater may mix is brackish transition-zone water derived in part from interaction of continental waters with the sedimentary aquifer. Isotopically, such continentally-derived fluids may resemble fluids originating from weathering of silicate-dominated terrains, consistent with our hypothesized fluid composition (von Strandman et al., 2008; 2010; Hindshaw et al., 2013). Given its plausibility alongside its ability to fit the observations, we favor this scenario to explain the geochemistry of the lower portion of the Coppercap Fm.

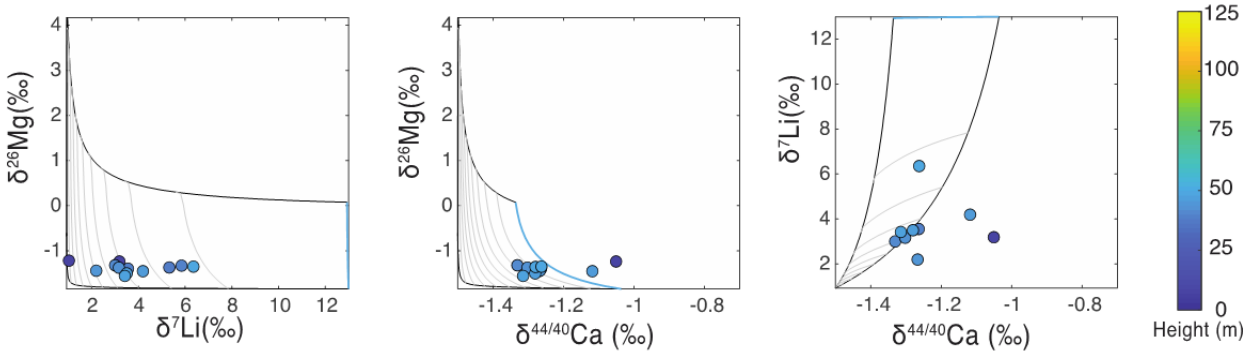

Figure S5: δ^{26}Mg - δ^7Li, δ^{26}Mg - $\delta^{44/40}$Ca and δ^7Li - $\delta^{44/40}$Ca cross-plots of both model solutions and data from the lower portion of the Coppercap Fm. The colours of data points represent stratigraphic height. Model solutions correspond to parameters presented in Table S6.

Table S6: Model parameters to explain the geochemistry of lower samples through a groundwater influence on the chemical and isotopic composition of the dolomitizing fluid.

Parameter	Definition	Value used in model
M_{fd}	Chemical composition of	Ca = 7.0, Mg = 15.1, Li =

	diagenetic fluid (mmol/kg)	0.0007
δ_{fd}	Isotopic composition of diagenetic fluid	$\delta^{44/40}$Ca = -0.98‰, δ^{26}Mg = 0.1‰, δ^{7}Li = 13.0 ‰
M_{fsw}	Chemical composition of seawater (mmol/kg)	Ca = 19.1, Mg = 43.2, Li = 0.002
M_s	Chemical composition of primary solid (aragonite)	Ca = 39.5%, C = 12%, Mg = 1.03%, Li = 0.03 ppm
δ_{fsw}	Isotopic composition of seawater	$\delta^{44/40}$Ca = 0.0‰, δ^{26}Mg = 0.1‰, δ^{7}Li = 13‰
δ_s	Isotopic composition of primary solid (aragonite)	$\delta^{44/40}$Ca = -1.5‰, δ^{26}Mg = -0.6‰, δ^{7}Li = 1‰
M_{fgw}	Chemical composition of groundwater (mmol/kg)	Ca = 0.5, Mg = 0.02, Li = 2 x 10^{-8}
δ_{fgw}	Isotopic composition of groundwater	$\delta^{44/40}$Ca = -1.5‰, δ^{26}Mg = -1.1‰, δ^{7}Li = 1.0‰
Ratio of seawater to groundwaters		0.35

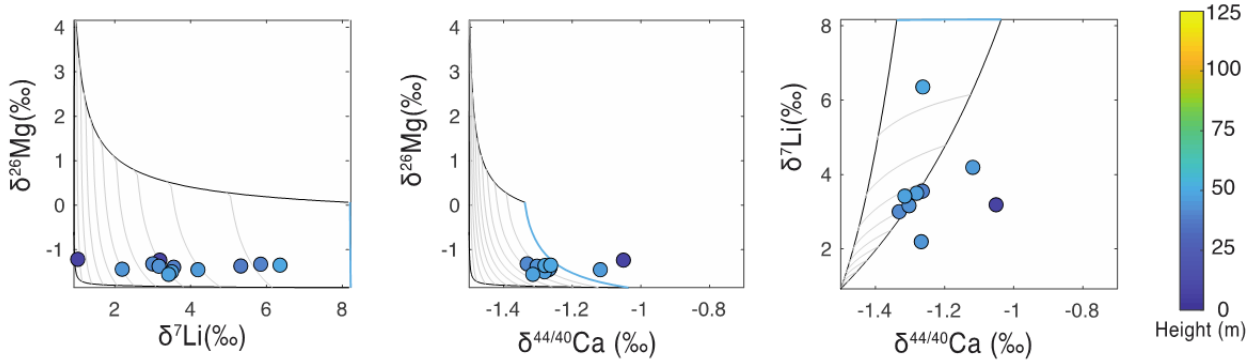

Figure S6 δ^{26}Mg - δ^{7}Li, δ^{26}Mg - $\delta^{44/40}$Ca and δ^{7}Li - $\delta^{44/40}$Ca cross-plots of both model solutions and data from the lower portion of the Coppercap Fm. The colours of data points represent stratigraphic height. Model solutions correspond to parameters presented in Table S7.

Table S7: Model parameters to explain the geochemistry of lower samples through a groundwater influence on the chemical and isotopic composition of the dolomitizing fluid.

Parameter	Definition	Value used in model
M_{fd}	Chemical composition of diagenetic fluid (mmol/kg)	Ca = 7.0, Mg = 15.4, Li = 0.00135
δ_{fd}	Isotopic composition of diagenetic fluid	$\delta^{44/40}$Ca = -0.98‰, δ^{26}Mg = 0.09‰, δ^{7}Li = 6.48 ‰
M_{fsw}	Chemical composition of seawater (mmol/kg)	Ca = 19.1, Mg = 43.2, Li = 0.002
M_s	Chemical composition of primary solid (aragonite)	Ca = 39.5%, C = 12%, Mg = 1.03%, Li = 0.03 ppm
δ_{fsw}	Isotopic composition of seawater	$\delta^{44/40}$Ca = 0.0‰, δ^{26}Mg = 0.1‰, δ^{7}Li = 13‰
δ_s	Isotopic composition of primary solid (aragonite)	$\delta^{44/40}$Ca = -1.5‰, δ^{26}Mg = -0.6‰, δ^{7}Li = 1‰

M_{fgw}	Chemical composition of groundwater (mmol/kg)	Ca = 0.5, Mg = 0.5, Li = 0.001
δ_{fgw}	Isotopic composition of groundwater	$\delta^{44/40}$Ca = -1.5‰, δ^{26}Mg = -0.2‰, δ^{7}Li = 3.0‰
Ratio of seawater to groundwaters		0.35

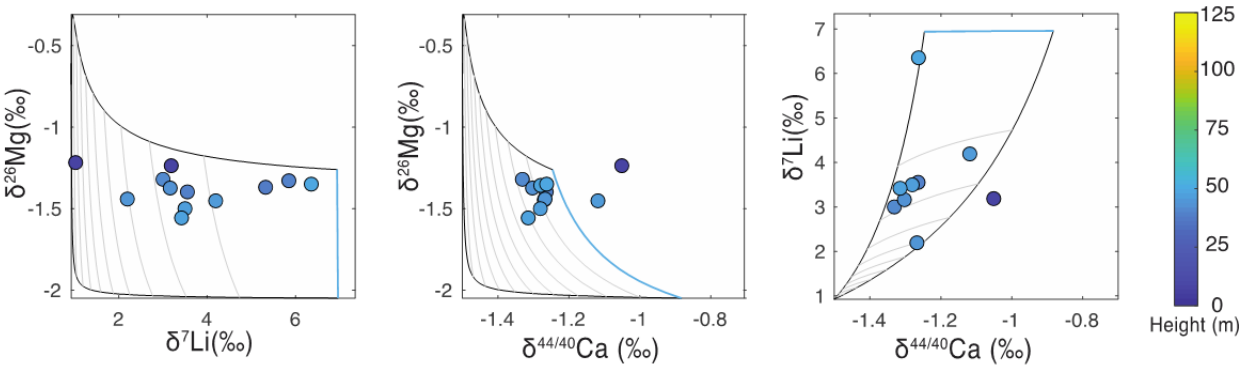

Figure S7: δ^{26}Mg - δ^{7}Li, δ^{26}Mg - $\delta^{44/40}$Ca and δ^{7}Li - $\delta^{44/40}$Ca cross-plots of both model solutions and data from the lower portion of the Coppercap Fm. The colours of data points represent stratigraphic height. Model solutions correspond to parameters presented in Table S8.

Table S8: Model parameters to explain the geochemistry of lower samples through a brackish transitional water influence on the chemical and isotopic composition of the dolomitizing fluid.

Parameter	Definition	Value used in model
M_{fd}	Chemical composition of diagenetic fluid (mmol/kg)	Ca = 10.0, Mg = 26.5, Li = 0.00125
δ_{fd}	Isotopic composition of diagenetic fluid	$\delta^{44/40}$Ca = -0.83‰, δ^{26}Mg = -0.08‰, δ^{7}Li = 6.96‰
M_{fsw}	Chemical composition of seawater (mmol/kg)	Ca = 19.1, Mg = 43.2, Li = 0.002
M_{s}	Chemical composition of primary solid (aragonite)	Ca = 39.5%, C = 12%, Mg = 1.03%, Li = 0.03 ppm
δ_{fsw}	Isotopic composition of seawater	$\delta^{44/40}$Ca = 0.0‰, δ^{26}Mg = 0.1‰, δ^{7}Li = 13‰
δ_{s}	Isotopic composition of primary solid (aragonite)	$\delta^{44/40}$Ca = -1.5‰, δ^{26}Mg = -0.6‰, δ^{7}Li = 1‰
M_{fgw}	Chemical composition of brackish transitional waters (mmol/kg)	Ca = 7.0, Mg = 21.0, Li = 0.001
δ_{fgw}	Isotopic composition of Brackish Transitional Waters	$\delta^{44/40}$Ca = -1.1‰, δ^{26}Mg = -0.2‰, δ^{7}Li = 3.0‰
Ratio of seawater to brackish transitional waters		0.25

Data table S9: Geochemical results.

Sample	d13C	d18O	d44/40 Ca vs SW	d26/24 Mg vs DSM 3	d7Li vs LSVEC	Mg (mol/mol Ca)	Sr (mmol/mol Ca)	Mn (mmol/mol Ca)	Li (µmol/mol Ca)
M303-6.0	-4.49	-3.50		-1.22	1.03	0.84	0.34	5.48	1.81
M303-6.8	-4.95	-3.77	-1.05	-1.24	3.19	0.84	0.42	5.37	8.78
M303-36.6	-3.24	-2.71		-1.37	5.32	0.97	0.20	0.50	1.42
M303-37.4	-3.22	-3.19	-1.26	-1.40	3.55	0.97	0.25	0.54	1.21
M303-38.3	-3.09	-3.08		-1.33	5.85	0.97	0.23	0.72	0.72
M303-40.5	-2.13	-2.82	-1.33	-1.32	3.00	1.00	0.17	0.90	7.47
M303-41.4	-2.07	-2.87	-1.27	-1.45		0.98	0.16	0.87	1.35
M303-42.5	-2.03	-2.54	-1.30	-1.37	3.16	0.96	0.18	1.56	1.15
M303-43.6	-1.64	-3.26	-1.27	-1.44	2.20	0.99	0.17	1.40	1.87
M303-44.8	-1.43	-1.82	-1.12	-1.45	4.19	1.02	0.16	1.58	1.82
M303-45.9	-0.39	-3.31	-1.28	-1.50	3.50	0.93	0.14	1.37	1.23
M303-46.7	-1.89	-0.91	-1.32	-1.56	3.42	0.99	0.16	0.77	2.14
M303-48	-0.44	-1.83	-1.28	-1.36		0.98	0.24	1.04	0.15
M303-49	0.30	-1.88	-1.26	-1.35	6.35	0.99	0.14	0.89	0.97
M303-50.3	0.37	-2.07	-1.20	-1.40		0.97	0.17	1.37	0.90
M303-51.1	-0.13	2.26	-1.18	-1.57	7.79	0.99	0.15	0.92	2.00
M303-52	0.63	0.78	-1.14	-1.50	7.88	0.97	0.15	1.33	1.65
M303-53.7	0.51	-2.08	-1.14	-1.39	8.46	1.01	0.15	1.84	2.42
M303-54.5	0.72	0.54	-1.12	-1.61	7.22	1.00	0.15	2.24	2.04
M303-55.9	0.13	0.48	-1.01	-1.95	8.92	1.00	0.13	1.27	2.05
M303-57	0.42	1.62	-0.98	-1.78	9.59	0.98	0.13	1.65	1.46
M303-57.9	0.43	1.40	-0.78	-1.66	9.51	1.00	0.12	1.34	1.15
M303-59.2	1.21	2.17	-0.86	-1.72	9.22	1.01	0.14	1.99	1.83
M303-59.9	0.60	-0.02		-1.61	9.19	1.02	0.14	1.33	1.88
M303-62.5	0.83	-1.74	-0.65	-1.67	9.73	1.00	0.12	1.31	1.28
M303-63.3	0.87	-4.16	-0.89	-1.50	8.27	1.00	0.15	1.87	1.77
M303-67.3	0.87	-0.49	-0.78	-1.59	9.62	1.01	0.12	1.81	1.90
M303-68	0.96	-3.26	-0.77	-1.41	7.91	1.00	0.13	1.92	1.70
M303-69	0.72	-2.57	-0.85	-1.68		1.04	0.18	2.32	1.76
M303-70.7	0.63	-5.62	-0.60	-1.80	8.68	1.03	0.17	1.01	1.67
M303-71.1	0.54	-4.22		-1.68	8.40	1.04	0.18	0.99	1.82
M303-72.6	0.44	-5.74	-0.25	-1.80	9.52	1.02	0.24	0.45	1.69
M303-73.6	0.96	-1.21	-0.37	-1.88	11.31	0.99	0.32	0.48	1.40
M303-74.6	1.05	-1.38	-0.55			1.01	0.28	0.67	1.56
M303-75.6	1.06	-2.52		-1.74		1.01	0.25	0.50	0.53
M303-76.6	0.86	-2.94	-0.48	-1.70	11.96	1.05	0.24	0.56	1.35
M303-77.7	0.55	-6.03	-0.82	-1.69	9.85	1.01	0.22	0.61	1.31
M303-79.3	0.86	-1.57	-0.71	-1.76	8.32	1.01	0.28	0.57	1.09
M303.80.2	0.69	-4.35	-0.61	-1.61	12.04	1.03	0.29	0.56	0.74
M303-81.6	1.14	-2.10	-0.56	-1.69	12.73	1.01	0.32	0.35	1.96
M303-83.1	1.27	-1.43	-0.41	-1.85	8.49	1.03	0.29	0.15	1.65
M303-84.4	1.14	-3.19	-0.70	-1.91	5.94	1.06	0.18	0.12	0.50
M303-86.6	-0.34	-3.23			10.68	1.00	0.23	0.20	2.29
M303-88.6	-0.26	-8.45	-0.93	-1.13	8.04	0.97	0.13	0.38	1.64
M303-90.1	-0.27	-9.85	-0.94	-1.14	6.35	0.99	0.14	0.95	1.55
M303-92.6	-0.07	-1.59	-0.85	-1.06	8.48	0.92	0.21	0.49	0.69
M303-93.6	0.90	-8.64	-0.72	-1.53	3.96	0.99	0.23	0.51	1.12
M303-94.6	1.36	-7.55	-0.55	-1.50		1.02	0.17	0.39	0.83
M303-96.2	0.67	-11.29	-0.83	-1.27	8.12	1.00	0.12	0.83	0.97
M303-97.9	0.37	-11.63	-0.94	-1.23	7.71	0.98	0.10	0.52	1.48
M303-99.5	1.09	-12.17	-1.13	-0.91		0.95	0.10	3.25	10.01
M303-100.6	1.21	-12.48	-0.90	-0.95	6.07	0.99	0.08	1.67	0.62
M303-101.9	0.70	-11.62	-0.92	-1.27	8.55	0.99	0.13	0.72	0.86
M303-102.8	0.40	-11.68	-0.85	-1.16		0.97	0.09	0.78	0.38

M303-104.3	2.49	-12.86	-1.03	-0.85	6.17	0.98	0.07	1.30	0.69
M303-105.6	3.06	-13.39	-0.77	-0.57	4.98	0.97	0.11	1.45	0.50
M303-106.3	2.70	-13.17	-1.09	-0.68		0.96	0.08	1.79	0.57
M303-107.7	2.75	-12.92	-1.07	-0.94	7.56	1.00	0.07	1.78	0.70
M303-109.4	1.26	-11.99	-0.93	-0.99	7.25	1.01	0.10	0.83	0.44
M303-110.6	1.02	-12.59	-0.90	-1.04	7.52	0.96	0.06	0.44	1.41
M303-111.5	2.24	-13.13	-1.13	-0.87	6.30	1.00	0.09	3.28	0.65
M303-113.4	3.49	-12.86	-0.97	-0.62	6.79	0.97	0.09	1.95	0.56
M303-115.6	3.84	-13.12	-1.12	-0.71	5.00	0.97	0.06	1.84	1.81
M303-117.6	3.35	-12.22	-0.83	-1.28	8.20	1.01	0.12	0.47	8.78
M303-118.8	3.51	-11.85	-0.83	-1.60	8.25	0.99	0.09	0.50	1.42
M303-123.1	0.58	-5.10	-0.96	-1.20	9.60	0.95	0.13	0.34	1.21
M303-125.1			-0.99	-1.20	7.35	0.98	0.10	0.60	0.72
M303-125.7			-0.70	-1.30	7.19	0.98	0.11	0.66	7.47

References:

1. Caro, G., Papanastassiou, D.A. and Wasserburg, G.J., 2010, 40K–40Ca isotopic constraints on the oceanic calcium cycle: Earth and Planetary Science Letters, 296(1-2), pp.124-132.
2. Young, E.D., Galy, A. and Nagahara, H., 2002, Kinetic and equilibrium mass-dependent isotope fractionation laws in nature and their geochemical and cosmochemical significance: Geochimica et Cosmochimica Acta, 66(6), pp.1095-1104.
3. Heuser, A. and Eisenhauer, A., 2008, The calcium isotope composition (δ44/40Ca) of NIST SRM 915b and NIST SRM 1486: Geostandards and Geoanalytical Research, 32(3), pp.311-315.
4. Ahm, A.S.C., Bjerrum, C.J., Blättler, C.L., Swart, P.K. and Higgins, J.A., 2018, Quantifying early marine diagenesis in shallow-water carbonate sediments: Geochimica et Cosmochimica Acta, 236, pp.140-159.
5. Higgins, J.A. et al., 2018, Mineralogy, early marine diagenesis, and the chemistry of shallow-water carbonate sediments: Geochimica et Cosmochimica Acta, 220, pp.512-534.
6. Dellinger, M., Hardisty, D.S., Planavsky, N.J., Gill, B.C., Kalderon-Asael, B., Asael, D., Croissant, T., Swart, P.K. and West, A.J., 2020, The effects of diagenesis on lithium isotope ratios of shallow marine carbonates: American Journal of Science, 320(2), pp.150-184.
7. Taylor, H., Kell-Duivestein, I., Farkas, J., Dietzel, M. and Dosseto, A., 2019, Lithium isotopes in dolostone as a palaeo-environmental proxy-an experimental approach: Climates of the Past (15) pp. 635-646
8. Langer, G., Sadekov, A., Thoms, S., Mewes, A., Nehrke, G., Greaves, M., Misra, S., Bijma, J. and Elderfield, H., 2015, Li partitioning in the benthic foraminifera A mphistegina lessonii: Geochemistry, Geophysics, Geosystems, 16(12), pp.4275-4279.
9. Langer, G., Sadekov, A., Greaves, M., Nehrke, G., Probert, I., Misra, S. and Thoms, S., 2020. Li partitioning into coccoliths of Emiliania huxleyi: evaluating the general role of "vital effects" in explaining element partitioning in biogenic carbonates: Geochemistry, Geophysics, Geosystems, 21(8), p.e2020GC009129.
10. Jacobson, A.D. and Holmden, C., 2008, δ44Ca evolution in a carbonate aquifer and its bearing on the equilibrium isotope fractionation factor for calcite: Earth and Planetary Science Letters, 270(3-4), pp.349-353.
11. Fantle, M.S. and DePaolo, D.J., 2007, Ca isotopes in carbonate sediment and pore fluid from ODP Site 807A: the Ca2+ (aq)–calcite equilibrium fractionation factor and calcite recrystallization rates in Pleistocene sediments: Geochimica et Cosmochimica Acta, 71(10), pp.2524-2546.
12. Fantle, M.S. and Higgins, J., 2014, The effects of diagenesis and dolomitization on Ca and Mg isotopes in marine platform carbonates: implications for the geochemical cycles of Ca and Mg: Geochimica et Cosmochimica Acta, 142, pp.458-481.
13. Horita, J., 2014, Oxygen and carbon isotope fractionation in the system dolomite–water–CO2 to elevated temperatures: Geochimica et Cosmochimica Acta, 129, pp.111-124.
14. Gussone, N., Ahm, A.S.C., Lau, K.V. and Bradbury, H.J., 2020, Calcium isotopes in deep time: Potential and limitations: Chemical Geology, p.119601.
15. Wang, Z., Hu, P., Gaetani, G., Liu, C., Saenger, C., Cohen, A. and Hart, S., 2013, Experimental calibration of Mg isotope fractionation between aragonite and seawater. Geochimica et Cosmochimica Acta, 102, pp.113-123.
16. Romanek, C.S., Grossman, E.L. and Morse, J.W., 1992, Carbon isotopic fractionation in synthetic aragonite and calcite: effects of temperature and precipitation rate: Geochimica et cosmochimica acta, 56(1), pp.419-430.
17. Dellinger, M., West, A.J., Paris, G., Adkins, J.F., von Strandmann, P.A.P., Ullmann, C.V., Eagle, R.A., Freitas, P., Bagard, M.L., Ries, J.B. and Corsetti, F.A., 2018, The Li isotope composition of marine biogenic carbonates: Patterns and Mechanisms: Geochimica et Cosmochimica Acta, 236, pp.315-335.
18. von Strandmann, P.A.P., Schmidt, D.N., Planavsky, N.J., Wei, G., Todd, C.L. and Baumann, K.H., 2019, Assessing bulk carbonates as archives for seawater Li isotope ratios: Chemical Geology, 530, p.119338.
19. Marriott, C.S., Henderson, G.M., Crompton, R., Staubwasser, M. and Shaw, S., 2004, Effect of mineralogy, salinity, and temperature on Li/Ca and Li isotope composition of calcium carbonate: Chemical Geology, 212(1-2), pp.5-15.
20. Fantle, M.S. and Tipper, E.T., 2014, Calcium isotopes in the global biogeochemical Ca cycle: Implications for development of a Ca isotope proxy: Earth-Science Reviews, 129, pp.148-177.
21. Swart, P.K., Ruiz, J. and Holmes, C.W., 1987. Use of strontium isotopes to constrain the timing and mode of dolomitization of upper Cenozoic sediments in a core from San Salvador, Bahamas: Geology, 15(3), pp.262-265.

22. Henderson, G.M., Slowey, N.C. and Haddad, G.A., 1999, Fluid flow through carbonate platforms: constraints from 234U/238U and Cl− in Bahamas pore-waters: Earth and Planetary Science Letters, 169(1-2), pp.99-111.
23. Macdonald, F.A., Schmitz, M.D., Crowley, J.L., Roots, C.F., Jones, D.S., Maloof, A.C., Strauss, J.V., Cohen, P.A., Johnston, D.T. and Schrag, D.P., 2010, Calibrating the Cryogenian: Science, 327(5970), pp.1241-1243.
24. Strauss, J.V., Rooney, A.D., Macdonald, F.A., Brandon, A.D. and Knoll, A.H., 2014, 740 Ma vase-shaped microfossils from Yukon, Canada: Implications for Neoproterozoic chronology and biostratigraphy: Geology, 42(8), pp.659-662.
25. Rooney, A.D., Macdonald, F.A., Strauss, J.V., Dudás, F.Ö., Hallmann, C. and Selby, D., 2014, Re-Os geochronology and coupled Os-Sr isotope constraints on the Sturtian snowball Earth: Proceedings of the National Academy of Sciences, 111(1), pp.51-56.
26. MacLennan, S., Park, Y., Swanson-Hysell, N., Maloof, A., Schoene, B., Gebreslassie, M., Antilla, E., Tesema, T., Alene, M. and Haileab, B., 2018, The arc of the Snowball: U-Pb dates constrain the Islay anomaly and the initiation of the Sturtian glaciation: Geology, 46(6), pp.539-542.
27. Berner, R.A. and Kothavala, Z., 2001, GEOCARB III: a revised model of atmospheric CO2 over Phanerozoic time: American Journal of Science, 301(2), pp.182-204.
28. McKenzie, N.R., Horton, B.K., Loomis, S.E., Stockli, D.F., Planavsky, N.J. and Lee, C.T.A., 2016, Continental arc volcanism as the principal driver of icehouse-greenhouse variability: Science, 352(6284), pp.444-447.
29. Ernst, R.E., Wingate, M.T.D., Buchan, K.L. and Li, Z.X., 2008. Global record of 1600–700 Ma Large Igneous Provinces (LIPs): implications for the reconstruction of the proposed Nuna (Columbia) and Rodinia supercontinents: Precambrian Research, 160(1-2), pp.159-178.
30. Lowenstein, T.K., Hardie, L.A., Timofeeff, M.N. and Demicco, R.V., 2003, Secular variation in seawater chemistry and the origin of calcium chloride basinal brines: Geology, 31(10), pp.857-860.
31. Horita, J., Zimmermann, H. and Holland, H.D., 2002, Chemical evolution of seawater during the Phanerozoic: Implications from the record of marine evaporites: Geochimica et Cosmochimica Acta, 66(21), pp.3733-3756.
32. Tipper, E.T., Lemarchand, E., Hindshaw, R.S., Reynolds, B.C. and Bourdon, B., 2012, Seasonal sensitivity of weathering processes: Hints from magnesium isotopes in a glacial stream: Chemical Geology, 312, pp.80-92.
33. Martin, A.N., Meredith, K., Norman, M.D., Bryan, E. and Baker, A., 2020, Lithium and strontium isotope dynamics in a carbonate island aquifer, Rottnest Island, Western Australia: Science of The Total Environment, 715, p.136906.
34. von Strandmann, P.A.P., Burton, K.W., James, R.H., van Calsteren, P., Gislason, S.R. and Sigfússon, B., 2008, The influence of weathering processes on riverine magnesium isotopes in a basaltic terrain: Earth and Planetary Science Letters, 276(1-2), pp.187-197.
35. von Strandmann, P.A.P., Burton, K.W., James, R.H., van Calsteren, P. and Gislason, S.R., 2010, Assessing the role of climate on uranium and lithium isotope behaviour in rivers draining a basaltic terrain: Chemical Geology, 270(1-4), pp.227-239.
36. Hindshaw, R.S., Reynolds, B.C., Wiederhold, J.G., Kretzschmar, R. and Bourdon, B., 2011, Calcium isotopes in a proglacial weathering environment: Damma glacier, Switzerland: Geochimica et Cosmochimica Acta, 75(1), pp.106-118.